

A Three-Dimensional Navier-Stokes Simulation of A Film-Cooled Turbine Stage

T. NISHIZAWA¹, K. SAIKI¹, O. NOZAKI¹, K. KIKUCHI¹

¹ Japan Aerospace Exploration Agency
7-44-1 Jindaiji-Higashi, Chofu, Tokyo 182-8522, Japan
Phone: +81-422-40-3424, Fax: +81-422-40-3438, E-mail: tn@nal.go.jp

ABSTRACT

Three-dimensional Navier-Stokes simulation is performed on the flow through a turbine stage with cooling air injection from multi-row holes on the surface of the stator vanes and the rotor blades. The computation is performed on a parallel computer with a very fine grid system, which has about thirty grid points inside each of cooling hole exits on the blade surface. The arrangements of the cooling holes, as well as the geometries of blades and passages, are given according to the real machine. The calculated result shows that the complicated three-dimensional flow structure in the stator and rotor passages, including secondary flow and flow separation on the end walls. It also shows how the injected coolant flows along the blade surfaces and how much the surface temperature is thereby lowered. A pair of kidney-shaped vortices is generated around cooling holes by the interaction between the coolant jet and the mainstream flow. The cooling effectiveness is estimated from the numerical result and compared with an empirical equation used for designing film-cooling arrangement. The influence of the coolant injection on the aerodynamic performance of turbine stage is also examined quantitatively.

NOMENCLATURE

Symbols

A	coefficient of empirical equation
B	coefficient of empirical equation
D	diameter of cooling hole
d	equivalent slot width of a row of cooling holes
Δh	spanwise hole spacing in a row
M	blowing ratio
V	flow velocity
P	pressure
Re	Reynolds Number
s	surface distance behind a cooling hole
T	temperature
X	non-dimensional distance
x	axial distance behind the trailing edge
Z	non-dimensional spanwise distance
z	spanwise distance
α	horizontal projection angle of coolant injection
β	vertical projection angle of coolant injection
η_f	film cooling effectiveness
ρ	fluid density
ω	total pressure loss

Subscripts

1	turbine inlet
2	turbine exit
a	adiabatic condition
c	coolant flow
g	mainstream gas
t	stagnation condition
w	on solid wall
∞	mainstream flow

INTRODUCTION

Steadily increasing turbine inlet temperature (TIT) of modern gas turbines has been achieved in order to realize more power and higher thermal efficiency. In recent years, the temperature is increased continuously by about 20 degrees a year in average and the research and development on ultra-high temperature gas turbines with TIT of about 1700 degrees centigrade are now in process. Most part of the increases of TIT has been achieved by some advanced air-cooling technologies, such as impingement cooling and film cooling. The total consumption of cooling air, which is bled out from the compressor passages and injected into the turbine passages, is on the upward trend as more advanced cooling technologies are used. One of the most important requirements is to reduce the coolant consumption as much as possible by applying the most effective cooling design. This is because the coolant injection of film cooling results inevitably in decrease of mainstream gas temperature, increase of loss in mixing with mainstream flow, and eventually decrease of gas turbine output. Excessive coolant consumption may bring decreases of overall efficiency of a gas turbine system. Gas turbine designers have to see how injected coolant flows along blade surfaces and to see if the temperature of blades exceeds the strength limits of the materials or not. Then the optimum arrangements of film-cooling injection have to be established.

A national project of "High Temperature Materials in the 21st Century" is in process in Japan since 1999, in which new advanced materials with very high temperature capabilities have been extensively investigated for those applications to high-temperature machinery such as gas turbines and aero-engines (Harada, 2001). It is important to evaluate the capabilities of newly developed materials under practical use conditions, whereas it is very costly if the real machines are manufactured for this purpose. In the HTM21 Project, a simplified simulation system called "Virtual Gas Turbine" has been developed to estimate, on a small accessible computer, the temperature capabilities of new materials as well as the performance of a gas turbine made with such materials (Yoshida, et al., 2000, Yoshida, et al., 2001, and Saeki, et al. 2001). At present, a medium scale gas turbine of 17MW class output power is adopted as the first model of the virtual gas turbine. As an extension of this work,

fundamental examinations are in process to provide three-dimensional information on fluid flow condition, heat transfer, strength and material properties for the first stage of the model turbine.

In the present study, a three-dimensional Navier-Stokes simulation has been performed for a film-cooled turbine stage of the above model of virtual gas turbine. The simulation includes the mainstream flow through the passages of stator and rotor as well as the cooling air injection from multi-row holes on the surfaces of stator vanes and rotor blades. The positions and sizes of all the cooling holes, i.e. eight rows with totally 196 holes on a stator vane and seven rows with totally 98 holes on a rotor blade, are arranged to meet those of the real turbine. This complex arrangement of cooling holes is modeled using a structured grid system with about 13,200,000 grid points totally for the stator and rotor. Each hole is discretized with 5x5 or 6x6 grid points in this grid system. The pressure and temperature data of injected coolant at cooling hole exits have also been given so as to meet the real design conditions. This computation has been performed within a practical CPU time on the parallel computer system of National Aerospace Laboratory. The calculated results have been visualized to see the flow patterns of injected coolant as well as temperature distribution and film cooling effectiveness on the blade surface. The influence of the coolant injection on the aerodynamic performance of turbine stage is also examined quantitatively. In the present paper, the numerical result of the stator is chiefly examined.

NUMERICAL PROCEDURE

Figure 1 shows the stator vane of the model turbine considered in the present study, which has film-cooling holes on the surface as indicated by blue spots. In the real machine, other cooling schemes, such as impingement cooling with insert structure, pin-fin cooling and injection at the trailing edge, and impingement and film cooling on the end walls, are also adopted for the stator vanes as shown in Fig. 2 (Hijikata, et al., 1990). These latter cooling schemes are, however, omitted in the present calculation because of the simplification. Table 1 shows the specification of the model turbine, and the numerical simulation was conducted based on this. Reynolds number based on the blade height, the absolute flow velocity at rotor exit is about 100,000. Table 2 shows the specification of film cooling applied to the model turbine. On the stator vane, five staggered rows of cooling holes are arranged around the leading edge, in addition one row on the suction side and two rows on the pressure side. Each hole has a cross section of round shape (cylindrical hole) with a diameter of 0.6 mm. Coolant air is injected from each hole in a direction specified with both horizontal and vertical projection angles, as indicated Table 2. For example, around the leading edge the blowing direction inclines toward mid-span portion ($\beta=\pm 45^\circ$) in a plane perpendicular to the blade surface ($\alpha=90^\circ$) and, while on both the pressure and suction sides the direction is toward the stator exit and horizontal ($\alpha=50^\circ$, $\beta=0^\circ$). The number of cooling holes is totally 191 on the stator vane. In the present calculation, structured grid system is applied to simplify the calculation procedure by expressing the blowing conditions with straightforward boundary conditions on the blade surface. Grid points are arranged at the intervals of about 0.1mm within each of cooling hole, so that the space resolution of about 6x6 can be applied for each hole. The total number of grid points is about 6,600,000 ($225*61*481$) for a single stator passage.

Total temperature, total pressure and blowing directions are specified at each cooling hole as boundary condition. Total temperature is fixed at 405 degrees centigrade at all the holes, while total pressure is given so that the amount of coolant flow meets the design flow condition shown in Table 1. The blowing velocity is calculated using local static pressure extrapolated from mainstream flow, and is thus non-uniform but in a constant direction within each hole. The blowing directions are given individually for each hole according to its geometric data shown in Table 2 (Hijikata 1990). Adiabatic boundary condition is imposed on the end walls and blade surfaces except cooling holes. The boundary condition at the turbine

inlet is given according to the real operating condition of the model turbine with average total temperature of 1700 K and total pressure of about 0.98 MPa. The distribution of the inlet total temperature due to the combustion chamber will be shown later in Fig. 3. The flow direction at the stator inlet and the static pressure at the rotor exit are imposed as shown in Table 1.

Similar treatments are also made concerning the rotor blade. Around the leading edge, the blowing direction inclines toward the casing ($\beta=55^\circ$) in a plane perpendicular to the blade surface ($\alpha=90^\circ$) and while it inclines toward the rotor exit and the casing ($\alpha=50^\circ$, $\beta=55^\circ$) on both the pressure and suction sides. In the real machine, other cooling schemes, such as return-flow cooling with internal turbulence promoter, pin-fin cooling and injection at the trailing edge, are also applied for the rotor blades as shown in Fig. 2 (Hijikata, et al., 1990). However, they are omitted again for simplification in the present calculation. The number of rotor blades has been modified to 92 from 96 of the real machine for computational convenience.

The present computational method has been applied so far to many examples of flows in turbine and compressor cascades by the authors (Nozaki, et al., 1999a, Nozaki et al., 1999b and Unno, et al., 2001). The Reynolds-averaged Navier-Stokes equations are discretized by the finite difference method using TVD scheme to the nonlinear convection terms proposed by Chakravarthy-Oscher (1978) for stabilization of computation. An algebraic turbulence model by Baldwin-Lomax (1978) is used to evaluate turbulence viscosity. The present computation applies averaging over one pitch in the circumferential direction on the boundary, which connects the stator and rotor regions to each other (Mixing Plane Method). This is because in the present paper concerned is the steady-state aerodynamic and thermal conditions of the film-cooled turbine stage, not the unsteady interaction between the two cascades.

The parallel computation is applied by dividing the computational region into sub-regions in the radial direction, which has the greatest number of grid points (481 points). Here, twenty-five sub-regions are used for each single passage of stator and rotor, and so the number of processor elements is fifty. The computation time is about fifty hours from the initial condition, which has been obtained by a calculation without any film cooling either in stator or rotor (Hereafter, this is called "uncooled" calculation).

RESULT AND DISCUSSIONS

Temperature on stator vane

Figure 3 shows the radial distributions of static temperature on the surface of stator vane (recovery temperature) obtained from the uncooled calculation. The total temperature at the turbine inlet is also shown, which is given as the inlet boundary condition based on the reference data of the model turbine (Hijikata, 1990). The mean and the maximum values of the inlet total temperature are 1418 degrees, and 1530 degrees, respectively. The surface temperature on the pressure side and around the leading edge is almost equal or slightly lower than the inlet total temperature, while it is lowered by 100-200 degrees near to the tip and hub on the suction side. Although the details are described later, this is because the fluid with lower temperature on the end wall comes in toward mid-span by the secondary flow (passage vortex).

Figure 4 shows static temperature distribution and limiting streamlines on the surfaces of stator vane and the hub wall, which has been obtained by CFD calculation of the film-cooled turbine stage. It is clearly seen that temperature on the vane surface becomes considerably lower by the coolant injected from cooling holes except tip region. On the pressure side of stator vane as shown in Fig. 4(a), the influence of secondary flow is not large and thereby the coolant from the two rows of cooling holes flows almost straight, or horizontal, toward the trailing edge. The surface temperature is thereby very high near the tip, because coolant does not come into this region. Slight curves and inclinations of the coolant flow trajectories towards the mid span are chiefly due to the radial

injections around the leading edge.

On the suction surface as shown in Fig. 4(b), the influence of secondary flow is relatively large near to the tip and hub, which is shown as streamlines coming inward from the end wall corners. This is mainly due to the passage vortices, which are generated by the flow in the end wall boundary layer from the pressure side of the adjacent vane toward the suction side of the vane considered. The streamlines on the hub wall also show this flow across the passage. Due to this secondary flow, the fluid on the casing wall comes down along the vane suction surface and thereby the temperature near tip is very high. This high-temperature region becomes gradually larger in area toward the trailing edge. Oppositely near the hub, the surface temperature is not so high, because the cool fluid comes up from the hub wall. Note that the inlet temperature is already lower near the end walls than mid-span portion, especially near the hub.

The influence of horseshoe vortex, which is generated around the leading edge near hub, is also seen in Fig. 4. The streamlines on the hub wall obviously shows that the flow separation according to the horseshoe vortex occurs in front of the vane and this separation line extends almost across the passage. However, the horseshoe vortex seem to have little influence on the flow, as well as the temperature, on the vane surface, since the height of the horseshoe vortex is very small around the leading edge. The influence of the passage vortex becomes more remarkable in the downstream part of the stator vane.

Figure 5(a) shows the distributions of static temperature in the cutting planes perpendicular to the vane surface (viewing in the downstream direction), at four different positions downstream of the row of cooling holes on the suction side. Figure 5(b) shows the vorticity component normal to the same cutting plane. The figures show the distributions over two intervals of the hole spacing, which is three times as long as their diameter D (see Table 2). The low temperature portion just behind the cooling holes ($s/D=2.0$) shows a distribution in the shape of a symmetric kidney. This temperature distribution is attributed to a pair of vortices with the directions opposite to each other as shown in Fig. 5(b), which is usually called "kidney vortex." The kidney vortex is generated due to the shear stress, which occurs around each of the coolant jet flow by the interaction with the mainstream flow. The shape of the kidney vortex pair becomes asymmetric gradually in the downstream direction ($s/D=5.5, 7.0$), and the positions of the vortex move away from the blade surface ($s/D=11.5$).

Figure 6 shows static temperature distributions in three cutting planes perpendicular to the blade surface behind one row of cooling holes around the leading edge and two rows on the pressure side, respectively. For the leading edge shown in Fig. 6(a), a single vortex in the counter-clockwise direction appears clearly behind each of the cooling holes. This vortex is generated also due to the interaction between the mainstream flow and the coolant jet flow, which inclines in the radial direction by 45 degrees, i.e. upper-right direction in Fig. 6(a). This radial blowing breaks the symmetry of the kidney vortex, mainly because of the interaction between the vortex and the surface boundary layer (Broichhausen, et. al, 1997). In this case, the counterclockwise part (left part) of a kidney vortex develops greatly, and the other part is not clearly seen in Fig. 6(a). Honami, et. al (1994) suggested that for full lateral injection, i.e. $\beta=90^\circ$, the other part of vortex would not develop at all, and the present numerical result agrees qualitatively with their suggestion. For the two rows on the pressure side shown in Fig. 6(b) and Fig. 6(c), the temperature shows almost kidney-shaped distributions, which are however slightly asymmetric compared with the suction side shown in Fig. 5.

Figure 7 shows the film-cooling effectiveness, which is obtained from the same computational result as above and shown on an unrolled two-dimensional surface of the stator vane. The cooling effectiveness is defined here as follows:

$$\eta_f = (T_g - T_{aw}) / (T_g - T_c) \quad (1)$$

The static temperature of mainstream flow T_g is taken as the temperature at the positions above the coolant flow along the vane

surface. In the regions near to the tip and hub, the figure shows the red color which means that no effect is obtained by the film cooling. The reason for this has been mentioned before. Although the cooling effectiveness is almost zero near the hub, the surface temperature is not too high in this region. As shown in Fig. 3 for the uncooled case, the surface temperature on the vane without film cooling has already been much lower near the hub than the other region. This figure also shows that the flow inclines inward from the end walls by the secondary flow on the suction side, while the effect of the secondary flow is small on the pressure side. The effect of the horseshoe vortex on the cooling effectiveness is also negligible. The average film-cooling effectiveness on the stator vane surface is estimated as 0.37. In the present calculation, the turbine inlet flow rate is about 29.8 kg/s and the total amount of the injected coolant from the pressure and suction surfaces is about 2.9 % of the mainstream flow rate (about 5.9 % if the design amount of coolant from the trailing edge is summed), which agrees well with the design condition. Figure 8 shows the detailed, zoom-up distribution of the film-cooling effectiveness around the cooling holes on the suction surface. The cooling effectiveness attenuates slowly toward the downstream along with the coolant flow convection, while it decreases quite rapidly to the both upper and lower sides.

Matsushita et al. (2000) proposed a formulation for two-dimensional distribution of film-cooling effectiveness around a single hole jet on a plane, based on a variety of reference data on published scientific documents and papers. This formulation is described as a function of dimensionless distances $X=s/(M_d)$ and $Z=z/D$ on the plane, as follows:

$$\eta_f(X,Z) = A \exp[-B(C-X-A)] / C \quad (2)$$

$$C = \{(X+A)^2 + Z^2\}^{1/2} \quad (3)$$

Here, s is the surface distance measured from the downstream edge of a cooling hole, M the blowing ratio defined by $\rho_c V_c / \rho_s V_{\infty}$, d the equivalent slot width for a row of cooling holes defined by $\pi D^2 / 4 \Delta h$. It was shown by Matsushita that the formulation gave a good agreement with the cooling effectiveness obtained from the experiment by Sasaki, et al (1978). The coefficients A and B , which are constant respectively, were determined so that the formulation can fit the experimental data by Sasaki. Furthermore, it was shown that, in case of a single row of cooling holes, the cooling effectiveness agrees well with that obtained from a simple superposition of the formulation for each hole.

Figure 9(a) and Fig. 9(b) shows the variation of the cooling effectiveness against the dimensionless distance X , which are obtained from the present calculation data. The figures show the results for some cooling holes at different span-wise positions of two rows on the pressure surface (downstream side) and the suction surface, respectively. The holes of each row are numbered sequentially from hub to tip. The positions of the holes can be seen in Fig. 7. In these figures, the curves with red solid circles show the approximation curves for hole #6. This curve is obtained by applying the above equation (2) to hole #6, and by super-positioning the values to the neighboring holes on the both sides, #5 and #7. On the pressure side, the formulation gives a good agreement with the numerical data. The curve for each hole is smoothly attenuated with the surface distance and at the same time the difference between holes is very small. On the other hands on the suction side, the formulation shows poor agreement with the numerical data. The numerical data do not show very smooth attenuation with surface distance and the differences among cooling holes are not small. Especially near the hub (hole #1) and tip (hole #32), the cooling effectiveness is considerably smaller than the other span positions. This is considered as the influence of the secondary flow near hub and tip on the suction side as mentioned before.

Aerodynamic loss behind stator

Figure 10 shows the total pressure distribution on x-constant

planes at two different axial positions, i.e. $x=0.1\text{mm}$ and $x=5\text{mm}$ behind the stator trailing edge. The figure shows the front views of the drawing planes over two blade pitches, though the calculation is performed only for one pitch. In Fig. 10(a), the vertically expanded narrow region with very small the total pressure, drawn by blue color, corresponds to the circumferential position of the wake immediately behind the trailing edge of stator vane. The total pressure loss in the wake region is large in a wider region on the suction side than the pressure side. Especially near the hub and casing on the suction side, the rolling-ups of fluid with large loss due to the passage vortices can be seen, which make the wake very thick. The mixing of the coolant with the mainstream flow in the boundary layer is enough on the suction side so that the individual jet flows cannot be observed, while the individual jets can be clearly observed on the pressure side. In Figure 10(b), though the mixing between the coolant and the mainstream flow proceeds further and the wake becomes wider and diffused than in Fig. 10(a). The influence of the passage vortices can be still observed near the end walls.

Figure 11 shows the distribution of total pressure loss against the tangential position on the mid-span height of the flow passage at the same axial positions as those in Fig. 10(a) and Fig. 10(b). The figure also shows the result for the uncooled case (indicated by "solid" in the figure) for the comparison. The total pressure loss is defined here as:

$$\omega = (P_{t1} - P_{t2}) / (P_{t1} - P_2) \quad (4)$$

In the case of film-cooled turbine stator as compared with uncooled one, the wake with large loss becomes wider in circumferential width and shifted to the suction side at the same time. The peak position moves circumferentially by about 6% of chord length at the axial position of $x=5\text{mm}$. The average total pressure loss at the same position becomes $\omega=0.092$, which is larger than the uncooled case by about 12%. The average whirl angle of flow behind the stator is about 76 degrees, which is almost the same as uncooled case. However, the center of the wake, if defined by the trajectory of the maximum peaks of the total pressure loss, inclines to the suction side by about 2.7 degrees as compared with uncooled case. These variations of aerodynamic characteristics can be considered as the effects of coolant injections from stator surface. Similar results on the variations, due to the cooling injections, in the aerodynamic characteristic of a turbine stator cascade have been reported by Saeki, et al. (1978) with detailed experimental examinations, which shows qualitatively the same trends as the present calculation.

Rotor

For the last part of the present paper, the flow condition in the rotor is briefly examined. Fig. 12 shows the temperature distribution and the limiting streamlines on the pressure and suction surfaces of rotor blades and the hub wall. The blowing direction of coolant from this rotor blade is always toward the outer casing and its vertical projection angle is fixed at 55 degrees for all the holes of the rotor.

Strong influences of the secondary flow inward from the end walls can be seen on the blade suction surface in Fig. 12(a), accompanying the flow separation in both the upper and lower regions. The separated regions begin just behind the leading edge and increase considerably in size to the trailing edge. These regions cover about twenty-five percent of the blade height, respectively. In these regions the flow comes down from the tip (or comes up from the hub) on the blade surface, and so most of coolant from the upstream holes does not come in. The film-cooling effectiveness is thereby expected to be small in these regions. The temperature in the upper separated region is higher than the other area covered by the coolant, because of high temperature fluid near the casing coming down. On the other hand, the temperature is low enough in the lower separated region near the hub. The inlet flow to the rotor has already low temperature near the hub and such low temperature fluid comes up to the lower separated region. Due to this strong secondary flow, the radial injection of coolant toward the tip does not seem very

effective at least on the suction surface of the rotor blade. On the pressure side of rotor blade, the flow shows rather complicated features (Fig. 12(b)). The streamlines incline toward the tip region in the upstream part of the pressure side, while they change the direction toward the trailing edge in the upper part and toward the hub in the lower part. On the hub wall, the influences of the horseshoe vortex and the passage vortex are recognized clearly by the streamlines in Fig. 12(c). It is qualitatively the same as the stator hub wall, and is more obvious mainly due to the high turning of the rotor. Further examinations on the effects of the blade rotation will be made in future by the authors.

CONCLUDING REMARKS

A three-dimensional Navier-Stokes simulation has been performed for a film-cooled turbine stage. The simulation includes the coolant injection from multi-row holes on the surfaces of the stator vanes and rotor blades. The positions and sizes of all the cooling holes are arranged to meet those of the real turbine. This complex arrangement of cooling holes is modeled using a structured grid system with very fine grid system, in which each hole is discretized with 5×5 or 6×6 grid points. The computations have been performed in a practical CPU time by using 50 processor elements on the super-parallel computer system. The pressure and temperature condition of coolant blowing at cooling holes have been prepared to meet the real conditions.

The numerical results have shown the complicated three-dimensional flow structures in the stator and rotor passages, including secondary flows, accompanying passage vortex and end-wall flow separations. It has been also shown how the injected coolant flows along blade surfaces and how it is related to the temperature distributions on the blade surfaces. Passage vortices have dominant effects on the overall flow pattern of injected air, i.e. the injected coolant tends to incline towards mid-span region according to the behavior of the passage vortices. A pair of kidney vortices is generated around each of coolant jet flow and they have large effects on the local flow patterns and the temperature distribution around cooling holes on blade surfaces. The influence of the coolant injection on the aerodynamic performance of the turbine stage has been also shown.

ACKNOWLEDGEMENT

The authors wish to pay the greatest respect to Dr. T. Yoshida, Dr. Y. Fukuyama, Dr. T. Yamane, and Dr. M. Matsushita of National Aerospace Laboratory, as well as Mr. T. Sasaki, and Y. Saeki of Toshiba Corporation for their kind contributions with many advises to proceed this study. Sponsorship for a significant portion of this work from the High Temperature Materials in the 21st Century (HTM21) Project by National Institute for Materials Science (NIMS) is greatly acknowledged.

REFERENCES

- Baldwin, B. and Lomax, H., 1978, "Thin-Layer Approximation and Algebraic Model for Separated Turbulent Flows," AIAA-78-0257.
- Broichhausen, K.-D. and Fritsch, G., 1997, "Systematic Study on the Fluid Dynamic Behaviour of Streamwise and Laterally Inclined Jets in Crossflow," ASME Paper 97-GT-98.
- Chakravathy, S.R. and Osher, S., 1985, "A New Class of High Accuracy TVD for Hyperbolic Conservation Laws", AIAA-85-0363.
- Harada, H., 2001, "High Temperature Materials 21 Project: Present Status and Plans for Future," Proceedings, High Temperature Materials 2001, organized by National Research Institute for Metals.
- Hijikata, T., Okamura, T., Fukuda, M., and Ito, S., 1990, "Cooling Characteristic of Turbine Airfoils from High-Temperature Gas Turbine Full-Scale Demonstrator Tests," Proceedings, Gas Turbine, 1990 Fall Conference of GTSJ, (in Japanese).
- Honami, S., Shizawa, T., and Uchuyama, A., 1994, "Behaviour of the Laterally Injected Jet in Film Cooling: Measurements of

Surface Temperature and Velocity/Temperature Field within the Jet,” Journal of Turbomachinery, No. 116.

Matsushita, M. and Yoshida, T., 2000, “Application of Turbine Cooling Performance to the Virtual Gas Turbine,” 2000 Fall Conference of GTSJ, (in Japanese).

Nozaki, O., Kikuchi, K., Nishizawa, T., Matsuo, Y., Hirai, K., and Kodama, H., 1999a, “Three-Dimensional Viscous Analysis of Rotor-Stator Interaction in a Transonic Compressor,” AIAA 99-0239.

Nozaki, O., Kikuchi, K., Nishizawa, and T., Matsuo, Y., 1999b, “Unsteady Three-Dimensional Viscous Flow Computations of Multiple- Blade-Row Interactions,” Proceedings of 14th ISABE.

Otomo, F., Nakata, Kubo, and Suga, 1997, “Aerodynamic Loss Measurements for Individual Film Cooling of Gas Turbine Nozzle Cascade,” 1997 Fall Conference of GTSJ, (in Japanese).

Sasaki, M., Takahara, K., Kumagai, T. and Hamano, M., 1978, “Film Cooling Effectiveness for Injection from Multi-Row Holes,” ASME Paper 78-GT-32.

Saeki, H., Fukuyama, Y., Harada, H., and Yoshida, T., 2001, “Development of a Virtual Turbine System for New Materials Design,” Proceedings, High Temperature Materials 2001, organized by National Research Institute for Metals.

Unno, M., Kodama, H., Nozaki, O., and Nishizawa, T., 2001, “unsteady Three-Dimensional Navier-Stokes Simulations of Fan-OGV-Strut-Pylon Interaction,” Proceedings of 15th ISABE.

Yoshida, T., Nozaki, O., Ogawa, A., Ro, Y., Nishizawa, T., Kikuchi, K., Zhou, F., Fujisawa, Y., and Matsushita, M., 2000, “Development of a Virtual Gas Turbine for Material Evaluation,” Proceedings, High Temperature Materials 2000, organized by National Research Institute for Metals.

Yoshida, T., Harada, H., Fukuyama, Y., Ogawa, A., Nozaki, O., Nishizawa, T., Matsushita, M., and Zhou, F., 2001, “Virtual Turbine: Its State of the Art and Advanced Works in the Project,” Proceedings, High Temperature Materials 2001, organized by National Research Institute for Metals.

Table 1 Specification of the model turbine

Stator

Exit Mach Number	0.8
Exit Re Number	100,000
Blade Chord	59 mm
Blade Height	59 mm
Number of Blades	48
Inlet Total Pressure	980,665 Pa
Inlet Ave. Total Temperature	1418 °C
Inlet Flow Angle	Axial direction
Coolant Temperature	405 °C
Coolant Flow Ratio	6.0 % of stage inlet flow

Rotor

Exit Static Pressure	490,333 Pa
Blade Chord	36 mm
Blade Height	59 mm
Number of Blades	96
Rotational Speed	10200 rpm
Inlet Ave. Total Temperature	1312 °C
Coolant Temperature	400 °C
Coolant Flow Ratio	4.5 % of stage inlet flow

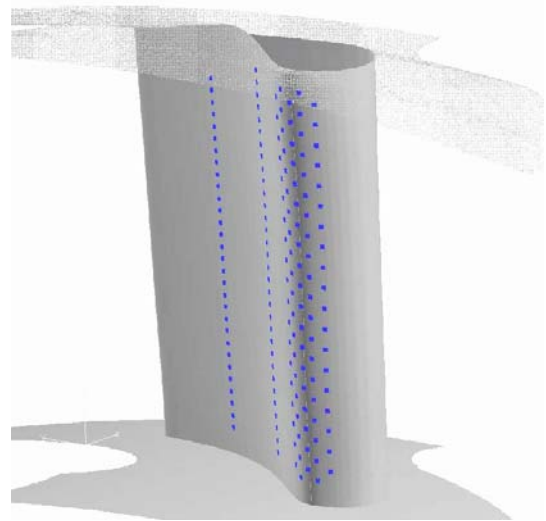
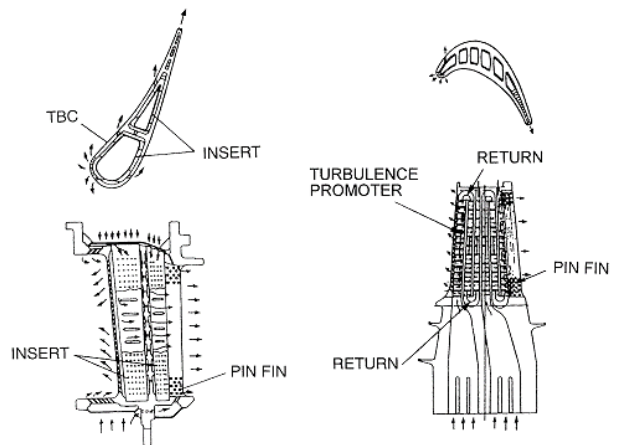


Fig. 1 Arrangement of film cooling holes on stator vane.

Table 2 Specification of cooling holes

Stator		Rotor	
L.E.	5 staggered rows	L.E.	4 staggered rows
D0.6x20 holes	$\Delta h: 3\text{mm}$ $\alpha: 90^\circ$ $\beta: \pm 45^\circ$	D0.5x24 holes	$\Delta h: 1.5\text{mm}$
		D0.5x12 holes	$\Delta h: 3\text{mm}$ $\alpha: 90^\circ$ $\beta: +55^\circ$
S.S.	1 row	S.S.	2 rows
D0.6x32 holes	$\Delta h: 1.8\text{mm}$ $\alpha: 50^\circ$ $\beta: 0^\circ$	D0.6x6-8holes	$\Delta h: 3\text{mm}$ $\alpha: 50^\circ$ $\beta: +55^\circ$
P.S.	2 rows	P.S.	1 row
D0.6x32 holes	$\Delta h: 1.8\text{mm}$ $\alpha: 50^\circ$ $\beta: 0^\circ$	D0.6x12 holes	$\Delta h: 3-5.4\text{mm}$ $\alpha: 40^\circ$ $\beta: +55^\circ$



(a) Stator vane (b) Rotor blade
Fig. 2 Cooling structure of model turbine.

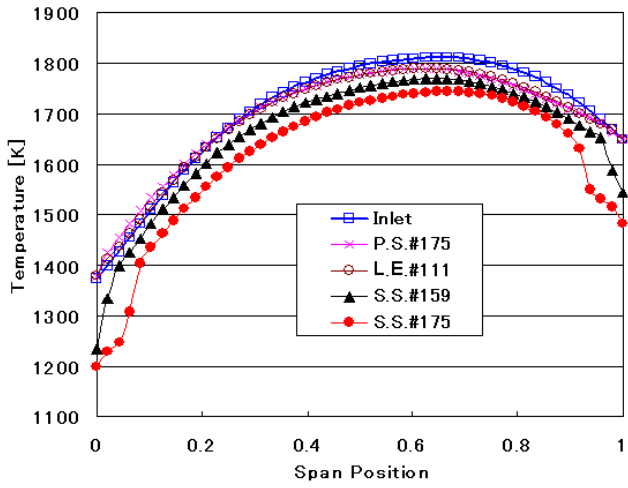


Fig. 3 Radial distribution of temperature in uncooled stator passage.

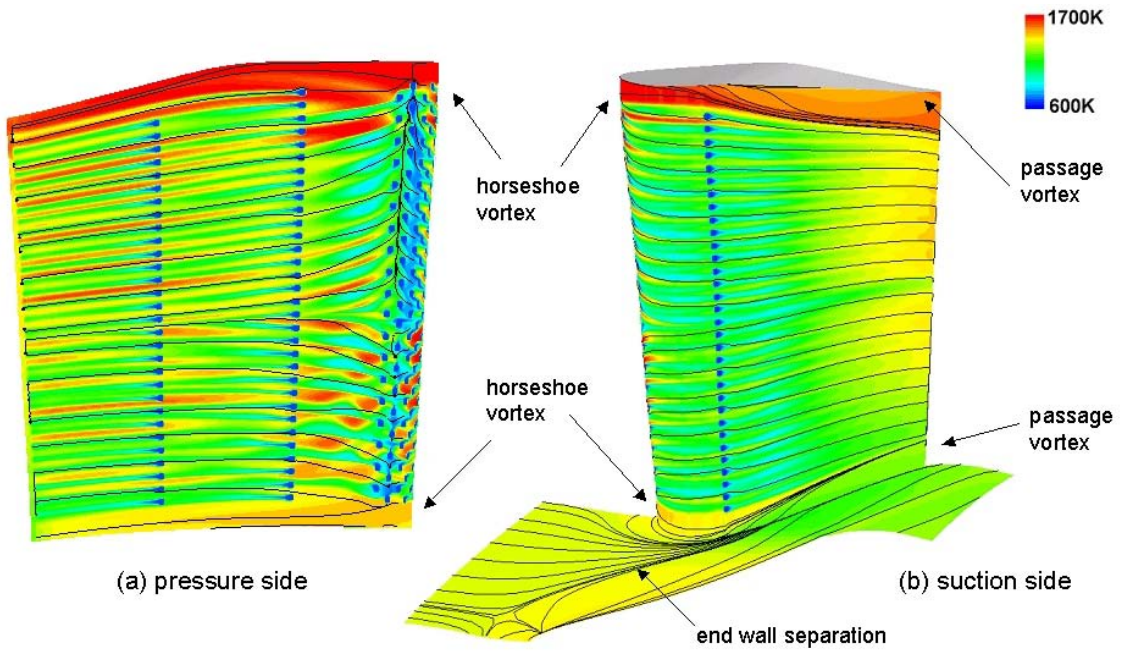
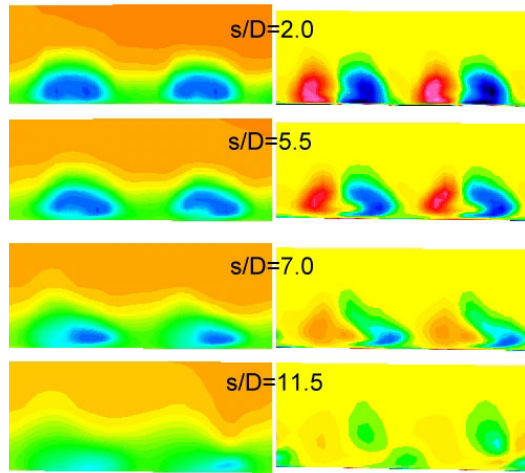


Fig. 4 Distribution of temperature and limiting streamlines on the surface of stator vane and hub wall.



(a) Static temperature (b) Vorticity

Fig. 5 Distribution of static temperature and vorticity component normal to the cutting plane perpendicular to the suction surface of stator vane. (viewing in the downstream direction)

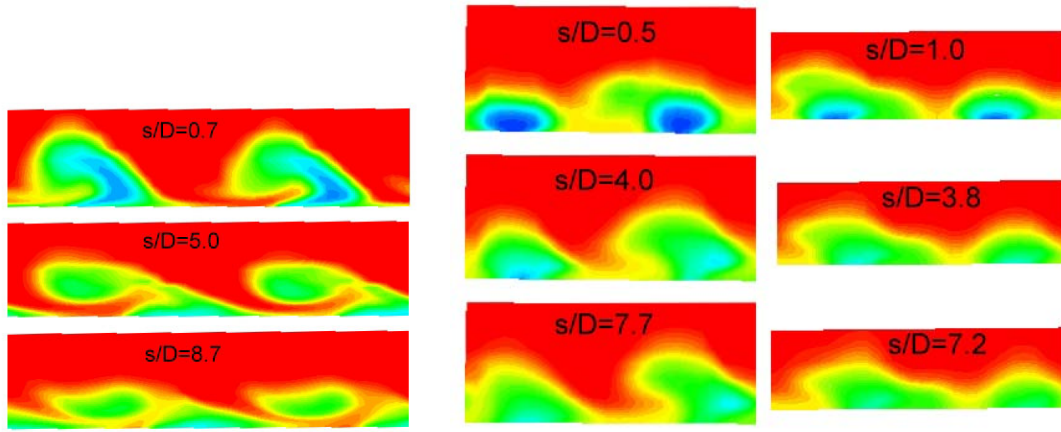


Fig. 6 Distribution of static temperature on the cutting plane perpendicular to the surface of stator vane near by leading edge, upstream and downstream on pressure surface (viewing in the downstream direction).

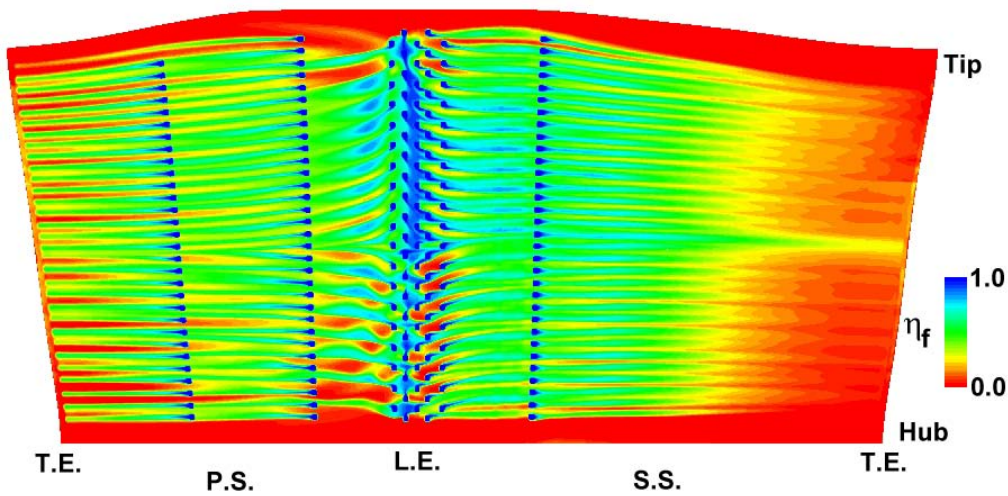


Fig. 7 Film cooling effectiveness on the surface of stator vane.

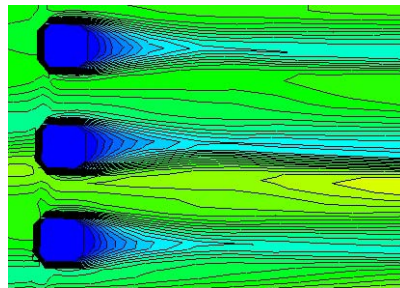
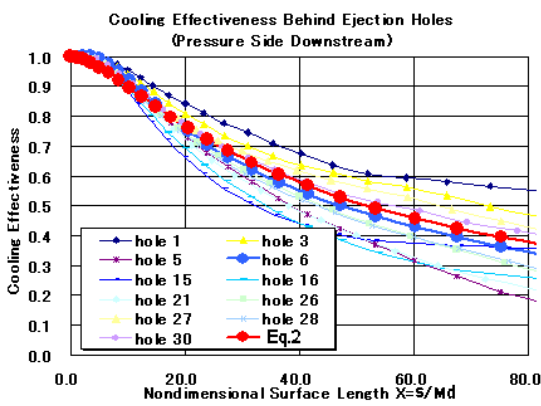
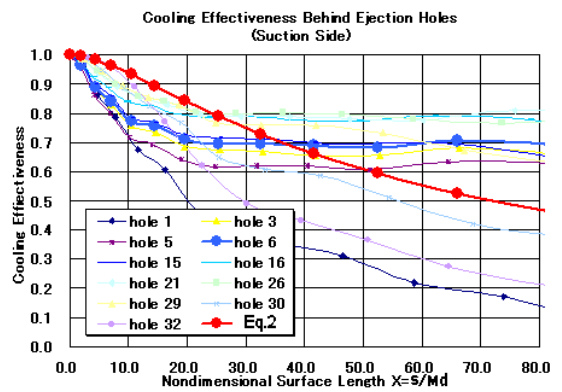


Fig. 8 Film cooling effectiveness around cooling holes on the suction surface of stator vane.

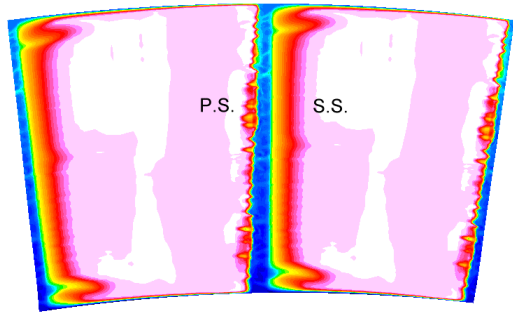


(a) Pressure surface (downstream side)

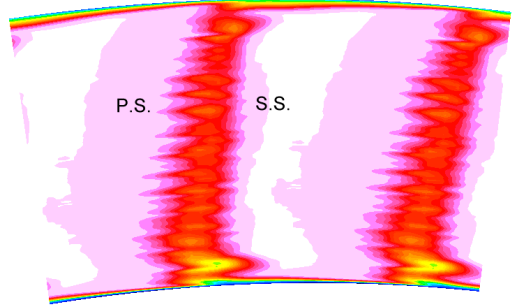


(b) Suction surface

Fig. 9 Approximation of film cooling effectiveness behind cooling holes on the pressure and suction surfaces of stator vane.



(a) Trailing edge (x=0.1mm)



(b) 8% chord downstream (x=5 mm)

Fig. 10 Total pressure distribution on x-constant planes in stator passage immediately behind (x=0.1mm) and 8% chord downstream (x=5 mm) of the trailing edge.

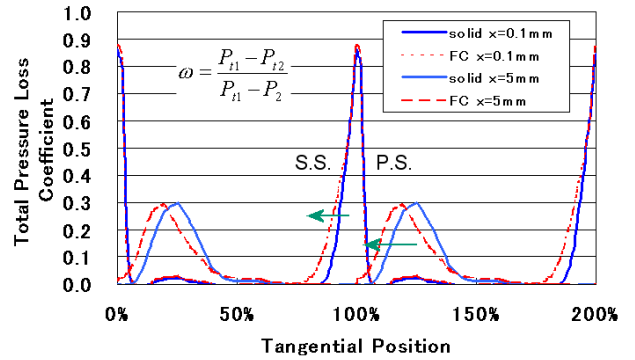
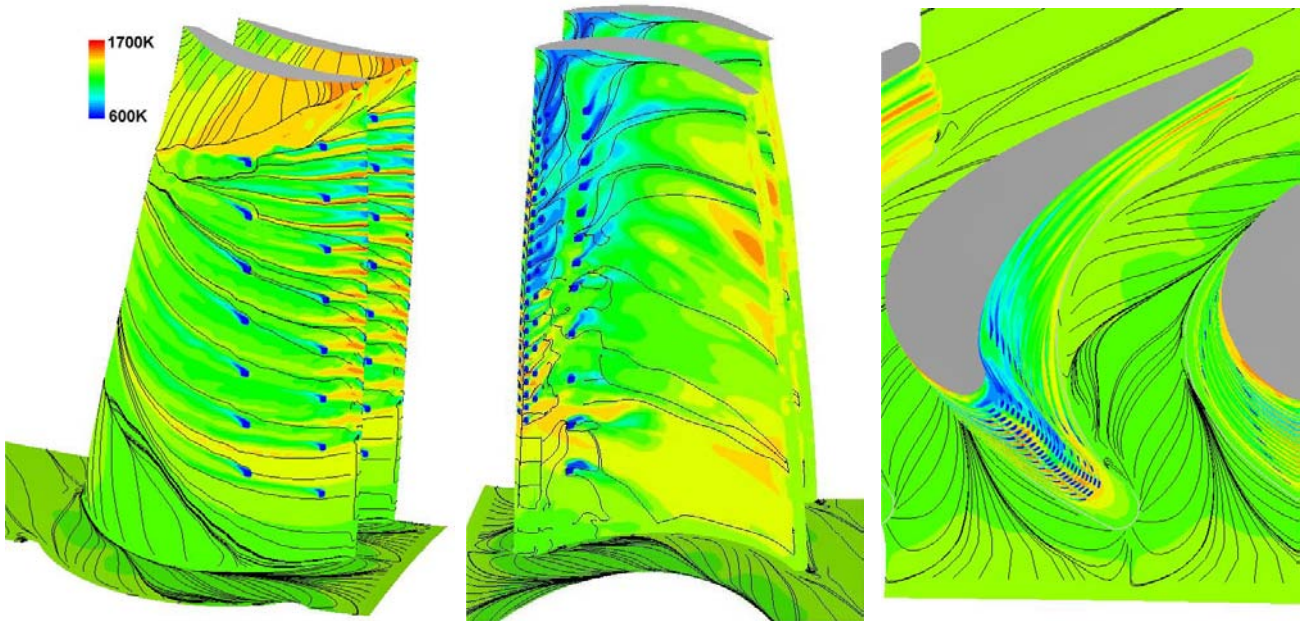


Fig. 11 Circumferential distribution of total pressure loss downstream of stator vane.



(a) Suction surface

(b) Pressure Surface

(c) Hub wall

Fig. 12 Distribution of temperature and limiting streamlines on the surface of rotor blade and hub wall.